

Copper-mediated thiol potentiation and mutagenesis-guided modeling suggest a highly conserved copper binding motif in human OR2M3

Franziska Haag¹, Lucky Ahmed², Krystle Reiss², Eric Block³, Victor S. Batista² and Dietmar Krautwurst¹

¹Leibniz-Institute for Food Systems Biology at the Technical University of Munich, Lise-Meitner-Str. 34, D-85354 Freising, Germany

²Department of Chemistry, Yale University, New Haven, CT 06520, United States

³Department of Chemistry, University at Albany, State University of New York, Albany, NY 12222, United States

Contents:

Table S1: Oligonucleotides for molecular cloning of odorant receptors investigated.....	2
Table S2: Oligonucleotides for <i>Homo sapiens</i> OR2M3 site-directed mutagenesis.	2
Table S3: Oligonucleotides for <i>Homo sapiens</i> OR2W1 site-directed mutagenesis.	4
Table S4: Vector internal oligonucleotides for pi2-dk (39aa rho-tag).	4
Table S5: NCBI reference sequences of olfactory receptor genes investigated.....	5
Table S6: EC ₅₀ values and relative amplitudes for 3-mercaptopentan-1-ol on OR2M3 wild type in the absence and presence of different heavy metals.	7
Table S7: EC ₅₀ values and relative amplitudes for OR2M3 wild type in the absence and presence of different concentrations of Cu ²⁺	7
Fig. S1. OR2M3 modeled 3-dimensional structure and its template.	8
Fig. S2. TMHMM posterior probabilities for OR2M3.	8
Fig. S3. OR2W1 and OR2M3 modeled 3-dimensional structures and their template.....	9
Fig. S4. TMHMM posterior probabilities for OR2W1.	9
Fig. S5. Ca-RMSD plot of OR2W1.	10
Fig. S6. Copper and silver enhance the 3-mercaptopentan-1-ol efficacy on OR2M3.	11
Fig. S7. The strongest increase in efficacy of 3-mercaptopentan-1-ol on OR2M3 was observed with 10 µmol/L Cu ²⁺	12
Fig. S8. Cu ²⁺ influences the efficacy of 3-mercaptopentan-1-ol on OR2M3 but not of OR2W1 agonists.	13
Fig. S9. SNP-defined OR2M3 haplotypes display 3-mercaptopentan-1-ol gain- and loss-of-function phenotypes.	14
Fig S10. Molecular models of the ligand and copper binding cavity for OR2M3.	15
Fig. S11. A conserved copper binding motif within OR2M3 homologs.	16
Fig. S12. Copper binding site within different ORs.	17
Fig. S13. Odorant binding site within different ORs.	18
Fig. S14: Cell surface expression of OR2M3 wt and variants.	19

Table S1: Oligonucleotides for molecular cloning of odorant receptors investigated.

Gene	Oligo-nucleotide	Restriction Site	TM (°C)		Sequence 5'→3'
hsOR1A1	344	Mfcl	66	fw	CGAT CAATTG ATG AGG GAA AAT AAC CAG TCC TCT ACA CTG GAA TTC ATC C
	cg-196	NotI	61	rv	CTGC <i>GC</i> GGCCGC TTA CGA GGA GAT TCT CTT GTT GAA GAG TTT CC
hsOR2M3	jf-071	Mfcl	64	fw	GTCG CAATTG ATG GCA AGG GAG AAT TCG ACC TTC AAC TCC G
	jf-072	NotI	63	rv	CTGC <i>GC</i> GGCCGC TCA CTC TCC AGA CTT GCC CTT TCC TAA GAT C
hsOR2W1	dk-807	EcoRI	58	fw	GTGA <i>GA</i> ATT C ATG GAC CAA AGC AAT TAT AGT TCT TTA CAT GG
	dk-808	NotI	59	rv	GCTAA <i>GC</i> GGCCGC CTA TGA CTT GCA ATT CCT CTT TAT TTT TGT AGA TTT G

TM = melting temperature, fw = forward, rv = reverse. Italic letters highlight the restriction sites. Start and Stop codons are bold.

Table S2: Oligonucleotides for *Homo sapiens* OR2M3 site-directed mutagenesis.

Gene	Oligonucleotide	TM (°C)		Sequence 5'→3'
OR2M3 Y ₁₀₄ C	FN-101	59	fw	<i>CAC AAA</i> TTT TCT TCT GTA CAT CAC TGC TTG G
	FN-102	60	rv	<i>GCA GTG</i> ATG TAC AGA AGA AAA TTT GTG TGG C
OR2M3 T ₁₀₅ A	FN-105	61	fw	<i>CAC AAA</i> TTT TCT TCT ATG CAT CAC TGC TTG GC
	FN-106	60	rv	<i>GCA GTG</i> ATG CAT AGA AGA AAA TTT GTG TGG C
OR2M3 T ₁₀₅ H	FN-051	59	fw	<i>CAA ATT</i> TTC TTC TAT CAC TCA CTG CTT GGC
	FN-052	60	rv	<i>CAG AGC</i> CAA GCA GTG AGT GAT AGA AG
OR2M3 T ₁₀₅ I	FN-103	60	fw	<i>CAA ATT</i> TTC TTC TAT ATA TCA CTG CTT GGC TCT G
	FN-104	60	rv	<i>GCC AAG</i> CAG TGA TAT ATA GAA GAA AAT TTG TGT G
OR2M3 T ₁₀₅ V	FN-191	59	fw	<i>CAC AAA</i> TTT TCT TCT ATG TAT CAC TGC TTG GC
	FN-192	58	rv	<i>CAA GCA</i> GTG ATA CAT AGA AGA AAA TTT GTG TG
OR2M3 G ₁₀₉ C	FN-053	58	fw	<i>CAT CAC</i> TGC TTT GCT CTG AAT GCT TTC
	FN-054	59	rv	<i>CAA AAG</i> AAA GCA TTC AGA GCA AAG CAG TG
OR2M3 G ₁₀₉ R	FN-131	61	fw	<i>CTA TAC</i> ATC ACT GCT TCG CTC TGA GTG C
	FN-132	60	rv	<i>GAA AGC</i> ACT CAG AGC GAA GCA GTG
OR2M3 C ₁₁₂ A	FN-047	59	fw	<i>GCT TGG</i> CTC TGA GGC CTT TCT TTT G
	FN-048	59	rv	<i>GCC AAA</i> AGA AAG GCC TCA GAG CC
OR2M3 C ₁₁₂ S	FN-049	58	fw	<i>GCT TGG</i> CTC TGA GAG CTT TCT TTT G
	FN-050	57	rv	<i>GCC AAA</i> AGA AAG CTC TCA GAG CC
OR2M3 M ₁₁₈ A	FN-235	61	fw	<i>CTT TTG</i> GCT GTT GCG GCT TAT GAC CG
	FN-236	64	rv	<i>GTA GCG</i> GTC ATA AGC CGC AAC AGC CAA AAG
OR2M3 D ₁₅₉ V	FN-133	59	fw	<i>CTA CGG</i> ATG GAA TTA TTG TTG TAG CAA C
	FN-134	60	rv	<i>CTA CAA</i> CAA TAA TTC CAT CCG TAG AGC C
OR2M3 C ₁₇₉ Y	FN-149	61	fw	<i>CCC ACT</i> TCT TCT ATG ACT TCC CCT CC
	FN-150	61	rv	<i>GTA GGG</i> AGG GGA AGT CAT AGA AGA AGT G
OR2M3 D ₁₈₀ E	FN-151	61	fw	<i>CCA CTT</i> CTT CTG TGA ATT CCC CTC CC
	FN-152	60	rv	<i>GTA GGG</i> AGG GGA ATT CAC AGA AGA AG
OR2M3 D ₁₈₀ N	FN-171	61	fw	<i>CCA CTT</i> CTT CTG TAA CTT CCC CTC CC
	FN-172	61	rv	<i>GAG GGG</i> AAG TTA CAG AAG AAG TGG GC

Table S2 continued

	FN-039	59	fw	GAA AAG ATT CTT TTC ATC AGC TGT ATA GTA ATG ATT G
OR2M3 C ₂₀₂ S	FN-040	59	rv	GAA AAC AAT CAT TAC TAT ACA GCT GAT GAA AAG AAT C
	FN-041	57	fw	GAT TCT TTT CAT CGC ATG TAT AGT AAT GAT TG
OR2M3 C ₂₀₂ A	FN-042	57	rv	GAA AAC AAT CAT TAC TAT ACA TGC GAT GAA AAG
	FN-045	58	fw	CTT TTC ATC TGC GCA ATA GTA ATG ATT GTT TTC
OR2M3 C ₂₀₃ A	FN-046	59	rv	GGG AAA ACA ATC ATT ACT ATT GCG CAG ATG
	FN-043	57	fw	GAT TCT TTT CAT CTG CAG TAT AGT AAT GAT TG
OR2M3 C ₂₀₃ S	FN-044	57	rv	GAA AAC AAT CAT TAC TAT ACT GCA GAT GAA AAG
	FN-107	58	fw	GAA AAG ATT CTT TTC ATC TGC TAT ATA GTA ATG ATT G
OR2M3 C ₂₀₃ Y	FN-108	59	rv	GGA AAA CAA TCA TTA CTA TAT AGC AGA TGA AAA GAA TC
	FN-241	58	fw	CTG CTG TAT AGT AGC GAT TGT TTT CCC
OR2M3 M ₂₀₆ A	FN-242	58	rv	CAG GGA AAA CAA TCG CTA CTA TAC AGC
	FN-109	59	fw	CAT CTG CTG TAT AGT AAT CAT TGT TTT CCC TG
OR2M3 M ₂₀₆ I	FN-110	61	rv	GCA ACA GGG AAA ACA ATG ATT ACT ATA CAG CAG
	FN-111	60	fw	CTG CTG TAT AGT AAT GCT GGT TTT CCC TG
OR2M3 I ₂₀₇ L	FN-112	60	rv	GCA ACA GGG AAA ACC AGC ATT ACT ATA CAG
	FN-237	60	fw	GCT TTT ACT ACT GCT TCC TCT CAC CTC
OR2M3 C ₂₄₁ A	FN-238	60	rv	GTG AGA GGA AGC AGT AGT AAA AGC TTT GC
	FN-239	61	fw	CTG CTT CCT CTG CCC TCT TGG TG
OR2M3 H ₂₄₄ A	FN-240	63	rv	CAC CAC CAA GAG GGC AGA GGA AGC
	FN-135	61	fw	GTA CTA TGG AGC AGG TTT GTT CAT GTA CAT AC
OR2M3 A ₂₅₅ G	FN-136	61	rv	GCC GTA TGT ACA TGA ACA AAC CTG CTC C
	FN-185	59	fw	GCA GCT TTG TTC ACG TAC ATA CGG C
OR2M3 M ₂₅₈ T	FN-186	61	rv	GTG GGC CGT ATG TAC GTG AAC AAA GC
	FN-197	60	fw	GTG TCT GTA TTC TGC ACC ATC CTC AC
OR2M3 Y ₂₇₈ C	FN-198	61	rv	GAG GAT GGT GCA GAA TAC AGA CAC CAT C
	FN-187	62	fw	CTC CCA TGT TGA ATT CCC TCA TCT ACA GC
OR2M3 P ₂₈₇ S	FN-188	60	rv	GAG GCT GTA GAT GAG GGA ATT CAA CAT G

TM = melting temperature, fw = forward, rv = reverse.

Table S3: Oligonucleotides for *Homo sapiens* OR2W1 site-directed mutagenesis.

Gen	Oligonucleotide	TM (°C)	Sequence 5'→3'
OR2W1 M ₁₀₅ H	FN-205	60	fw CTC TAT GTT TAC CAC TGG TTG GGC TC
	FN-206	60	rv CAA CTC TAT GTT TAC CAC TGG TTG GGC
OR2W1 S ₁₀₉ A	FN-253	60	fw GTG GTT GGG CGC AGT TGA GTG C
	FN-254	61	rv GAA GGC ACT CAA CTG CGC CCA AC
OR2W1 S ₁₀₉ C	FN-203	60	fw GTG GTT GGG CTG CGT TGA GTG C
	FN-204	59	rv CTC AAC GCA GCC CAA CCA CAT G
OR2W1 C ₁₁₂ A	FN-201a	61	fw GCT CAG TTG AGG CCC TTC TCC TG
	FN-202a	60	rv GCC AGG AGA AGG GCC TCA ACT G
OR2W1 C ₁₇₉ A	FN-207	60	fw GAT CAT TTC TTG GCT GAG TTG CCA GC
	FN-208	61	rv CAG AGC TGG CAA CTC AGC CAA GAA ATG
OR2W1 L ₂₀₂ C	FN-209	59	fw CTG TTT TCG CTT CGC GCA TTA TAA TTG TC
	FN-210	60	rv GAC AAT TAT AAT GCC GCA AGC GAA AAC AGA C
OR2W1 L ₂₀₂ S	FN-211	59	fw CTG TTT TCG CTT CCG GCA TTA TAA TTG TC
	FN-212	60	rv GAC AAT TAT AAT GCC GGA AGC GAA AAC AGA C
OR2W1 L ₂₀₂ C/G ₂₀₃ C	FN-243	61	fw GTC TGT TTT CGC TTG CTG CAT TAT AAT TGT CC
OR2W1 C ₂₄₁ A	FN-244a	61	rv GTG AGG ACA ATT ATA ATG CAG CAA GCG AAA AC
OR2W1 C ₂₄₁ A	FN-245	57	fw GCA ATG AAT ACC GCG GGA TCT C
	FN-246	58	rv GAT CCC GCG GTA TTC ATT GCT TTT C
OR2W1 H ₂₄₄ A	FN-247	58	fw CTG TGG ATC TGC TCT TAC TGT AGT G
	FN-248	58	rv GAC ACT ACA GTA AGA GCA GAT CCA C
OR2W1 Y ₂₅₂ A	FN-249	59	fw GTC TAT GTT CGC CGG AAC TAT TAT CTA C
	FN-250	58	rv GAT AAT AGT TCC GGC GAA CAT AGA CAC
OR2W1 Y ₂₅₉ A	FN-251	58	fw CTA CAT GGC CCT GCA ACC AGG
	FN-252	61	rv GTT ACC TGG TTG CAG GGC CAT GTA G
OR2W1 D ₂₉₆ N	FN-199	59	fw CAC CTT AAG AAA TAA GAA CAT GAA GGA TGC C
	FN-200	59	rv CAG GGC ATC CTT CAT GTT CTT ATT TCT TAA G

TM = melting temperature, fw = forward, rv = reverse.

Table S4: Vector internal oligonucleotides for pi2-dk (39aa rho-tag).

Oligonucleotide	TM (°C)		Sequence 5'→3'
dk-231	57 °C	fw	GCA GAG CTG GTT TAG TGA ACC G
dk-232a	59 °C	rv	GCA AGT AAA ACC TCT ACA AAT GTG GTA TGG

TM = melting temperature, fw = forward, rv = reverse

Table S5: NCBI reference sequences of olfactory receptor genes investigated.

Gene Description	Species	Common Species Name	NCBI Reference Sequence (Accession-number)
OR2M3	<i>Ailuropoda melanoleuca</i>	Giant panda	XM_002930259.1
OR2M3-like	<i>Aotus nancymaae</i>	Nancy Ma's night monkey	XM_012472652.1
OR2M3-like	<i>Bison bison bison</i>	Plains bison	XM_010861634.1
OR2M3-like	<i>Bos mutus</i>	Wild yak	XM_014480762.1
OR2M3	<i>Bos taurus</i>	Cattle	XM_015472178.1
OR2M3-like	<i>Canis lupus familiaris</i>	Domestic dog	XM_014118893.1
OR2M3-like	<i>Capra hircus</i>	Domestic goat	XM_013965440.2
OR2M3-like	<i>Cavia porcellus</i>	Guinea pig	XM_003479747.1
OR2M3	<i>Ceratotherium simum simum</i>	Southern white rhinoceros	XM_014797638.1
OR2M3	<i>Cercopithecus atys</i>	Sooty mangabey	XM_012045212.1
OR2M3-like	<i>Chlorocebus sabaeus</i>	Green monkey	XM_007990109.1
OR2M3-like	<i>Chrysochloris asiatica</i>	Cape golden mole	XM_006877082.1
OR2M3-like	<i>Colobus angolensis palliatus</i>	Angola colobus	XM_011955784.1
OR2M3	<i>Dipodomys ordii</i>	Ord's kangaroo rat	XM_013015457.1
OR2M3-like	<i>Echinops telfairi</i>	Lesser hedgehog tenrec	XM_004696864.2
OR2M3-like	<i>Equus asinus</i>	Asses	XM_014851596.1
OR2M3-like	<i>Equus caballus</i>	Domestic horse	XM_001493883.2
OR2M3-like	<i>Erinaceus europaeus</i>	European hedgehog	XM_007516422.1
OR2M3	<i>Felis catus</i>	Domestic cat	XM_011283070.2
OR2M3-like	<i>Galeopterus variegatus</i>	Malayan flying lemur	XM_008590481.1
OR2M3	<i>Gorilla gorilla gorilla</i>	Western lowland gorilla	XM_004028736.2
OR2M3	<i>Homo sapiens</i>	Human	NM_001004689.1
OR2M3-like	<i>Ictidomys tridecemlineatus</i>	Thirteen-lined ground squirrel	XM_005342365.1
OR2M3-like	<i>Loxodonta africana</i>	African bush elephant	XM_003423106.2
OR2M3	<i>Macaca fascicularis</i>	Crab-eating macaque	XM_005541090.2
OR2M3	<i>Macaca mulatta</i>	Rhesus macaque	XM_001094325.3
OR2M3	<i>Macaca nemestrina</i>	Southern pig-tailed macaque	XM_011729605.1
OR2M3	<i>Mandrillus leucophaeus</i>	Drill	XM_011972074.1
OR2M3	<i>Microcebus murinus</i>	Gray mouse lemur	XM_012758105.1
Olf164	<i>Mus musculus</i>	Mouse	NM_146451.1
OR2M3-like	<i>Nannospalax galili</i>	Mole rats	XM_008843779.1
OR2M3-like	<i>Orycteropus afer afer</i>	Aardvark	XM_007957565.1
OR2M3	<i>Otolemur garnettii</i>	Small-eared greater galago	XM_003803649.2
OR2M3-like	<i>Ovis aries</i>	Domestic sheep	XM_004008749.3
OR2M3	<i>Pan paniscus</i>	Bonobo	XM_003815318.2
OR2M3	<i>Pan troglodytes</i>	Common chimpanzee	XM_001143601.5
OR2M3	<i>Papio anubis</i>	Olive baboon	XM_003893634.2
OR2M3-like	<i>Propithecus coquereli</i>	Coquerel's sifaka	XM_012647451.1
Olf1570	<i>Rattus norvegicus</i>	Rat	NM_001000041.1
OR2M3	<i>Sus scrofa</i>	Wild boar	XM_013991466.1
OR2M3-like	<i>Tarsius syrichta</i>	Philippine tarsier	XM_008056882.1
OR2M3	<i>Tupaia chinensis</i>	Chinese tree shrew	XM_006165337.1
OR2M3	<i>Ursus maritimus</i>	Polar bear	XM_008710276.1
Olf165	<i>Mus musculus</i>	Mouse	NM_146466.1
Olf31	<i>Mus musculus</i>	Mouse	NM_147027.2

Table S5 continued

Olfr331	<i>Mus musculus</i>	Mouse	NM_001011861.3
Olfr330	<i>Mus musculus</i>	Mouse	NM_146879.2
Olfr325	<i>Mus musculus</i>	Mouse	NM_207153.2
Olfr328	<i>Mus musculus</i>	Mouse	NM_146502.2
Olfr224	<i>Mus musculus</i>	Mouse	NM_207695.1
Olfr720	<i>Mus musculus</i>	Mouse	NM_146392.1
Olfr314	<i>Mus musculus</i>	Mouse	NM_001011760.2
Olfr56	<i>Mus musculus</i>	Mouse	NM_010999.3
Olfr1396	<i>Mus musculus</i>	Mouse	NM_146337.1
Olr1606	<i>Rattus norvegicus</i>	Rat	NM_001000502.1
Olr1605	<i>Rattus norvegicus</i>	Rat	NM_001000088.1
Olr1425	<i>Rattus norvegicus</i>	Rat	NM_001000010.1
Olr1424	<i>Rattus norvegicus</i>	Rat	NM_001000779.1
Olr1607	<i>Rattus norvegicus</i>	Rat	NM_001000534.1
Olr1456	<i>Rattus norvegicus</i>	Rat	NM_001000956.1
Olr1386	<i>Rattus norvegicus</i>	Rat	NM_214834.1
Olr1384	<i>Rattus norvegicus</i>	Rat	NM_001002291.1
Olr1383	<i>Rattus norvegicus</i>	Rat	NM_214832.1
Olr1385	<i>Rattus norvegicus</i>	Rat	NM_214833.1
OR2T1	<i>Bos taurus</i>	Cattle	XM_002689121.2
OR2T2	<i>Bos taurus</i>	Cattle	XM_024995371.1
OR2T6	<i>Bos taurus</i>	Cattle	XM_002689120.2
OR2T8	<i>Bos taurus</i>	Cattle	XM_002689092.5
OR2T8	<i>Bos taurus</i>	Cattle	XM_002689090.3
OR2T11	<i>Bos taurus</i>	Cattle	XM_002689105.4
OR2T12	<i>Bos taurus</i>	Cattle	XM_005209254.3
OR2T27	<i>Bos taurus</i>	Cattle	XM_002689122.1
OR2T29	<i>Bos taurus</i>	Cattle	XM_010807207.3
OR2T33	<i>Bos taurus</i>	Cattle	XM_002689091.2
OR2V1	<i>Bos taurus</i>	Cattle	XM_002689049.2
OR2V2	<i>Bos taurus</i>	Cattle	XM_002689052.5
OR2M4	<i>Pan troglodytes</i>	Common chimpanzee	XM_016951697.2
OR2M5	<i>Pan troglodytes</i>	Common chimpanzee	XM_016951673.1
OR2T1	<i>Pan troglodytes</i>	Common chimpanzee	XM_003308851.1
OR2T2	<i>Pan troglodytes</i>	Common chimpanzee	XM_016948111.2
OR2T4	<i>Pan troglodytes</i>	Common chimpanzee	XM_001142557.2
OR2T6	<i>Pan troglodytes</i>	Common chimpanzee	XM_016951722.1
OR2T11	<i>Pan troglodytes</i>	Common chimpanzee	XM_525162.4
OR2T12	<i>Pan troglodytes</i>	Common chimpanzee	XM_001143155.4
OR2T27	<i>Pan troglodytes</i>	Common chimpanzee	XM_525157.5
OR2T29	<i>Pan troglodytes</i>	Common chimpanzee	XM_525160.6
OR2V1	<i>Pan troglodytes</i>	Common chimpanzee	XM_016953414.2
OR2V2	<i>Pan troglodytes</i>	Common chimpanzee	XM_016953415.1
OR2T1	<i>Canis lupus familiaris</i>	Domestic dog	XM_005628360.1
OR2T2	<i>Canis lupus familiaris</i>	Domestic dog	XM_539359.3
OR2T6	<i>Canis lupus familiaris</i>	Domestic dog	XM_844720.2
cOR2T18	<i>Canis lupus familiaris</i>	Domestic dog	NM_001256452.1

Table S5 continued

OR2T27	<i>Canis lupus familiaris</i>	Domestic dog	XM_539358.3
OR2T29	<i>Canis lupus familiaris</i>	Domestic dog	XM_539362.3
OR2T33	<i>Canis lupus familiaris</i>	Domestic dog	XM_003431849.1
cOR2T15	<i>Canis lupus familiaris</i>	Domestic dog	XM_539347.3
cOR2T24	<i>Canis lupus familiaris</i>	Domestic dog	XM_539346.3
cOR2T13	<i>Canis lupus familiaris</i>	Domestic dog	XM_539348.4
OR2V1	<i>Canis lupus familiaris</i>	Domestic dog	XM_548792.3

Table S6: EC₅₀ values and relative amplitudes for 3-mercaptopentan-1-ol on OR2M3 wild type in the absence and presence of different heavy metals.

Metal	EC ₅₀ in μmol/L ^a	Relative amplitude ^b
w/o	0.45 ± 0.19	1
CuCl ₂	0.55 ± 0.01	2.62 ± 0.80 ^c
CuCl ₂ + TEPA	1.13 ± 0.36	0.21 ± 0.03
CuCl ₂ ^d	0.25 ± 0.19	1
FeCl ₃	1.67 ± 0.34	1.04 ± 0.16
NiCl ₂	1.09 ± 0.63	0.50 ± 0.12
CoCl ₂	0.73 ± 0.26	0.40 ± 0.11
ZnSO ₄	n.d.	n.d.
AgAc	0.87 ± 0.50	5.72 ± 0.42
AgNO ₃	1.49 ± 0.36	6.41 ± 1.17
colloidal Ag	0.76 ± 0.35	3.52 ± 0.69

^amean ± SD (n=3-5). ^bData were normalized to the OR2M3 wt signal in response to 3-mercaptopentan-1-ol (20 μmol/L), measured in the absence of Cu²⁺. ^cOR2M3 wt with 3-mercaptopentan-1-ol (6 μmol/L). ^dOR2T11 C₁₁₉R with 2-methylpropane-2-thiol. n.d., no detectable response up to 60 μmol/L.

Table S7: EC₅₀ values and relative amplitudes for OR2M3 wild type in the absence and presence of different concentrations of Cu²⁺.

Copper concentration	EC ₅₀ in μmol/L ^a	Relative amplitude ^b
w/o	0.45 ± 0.19	1
10 μmol	0.29 ± 0.10	3.47 ± 1.90
30 μmol	0.55 ± 0.01	2.62 ± 0.80 ^c
60 μmol	1.47 ± 0.12	1.42 ± 0.64
100 μmol	1.95 ± 0.30	0.73 ± 0.48
300 μmol	n.d.	n.d.

^amean ± SD (n=3-5). ^bData were normalized to the OR2M3 wt signal in response to 3-mercaptopentan-1-ol (20 μmol/L), measured in the absence of Cu²⁺. ^cOR2M3 wt with 3-mercaptopentan-1-ol (6 μmol/L). n.d., no detectable response up to 60 μmol/L.

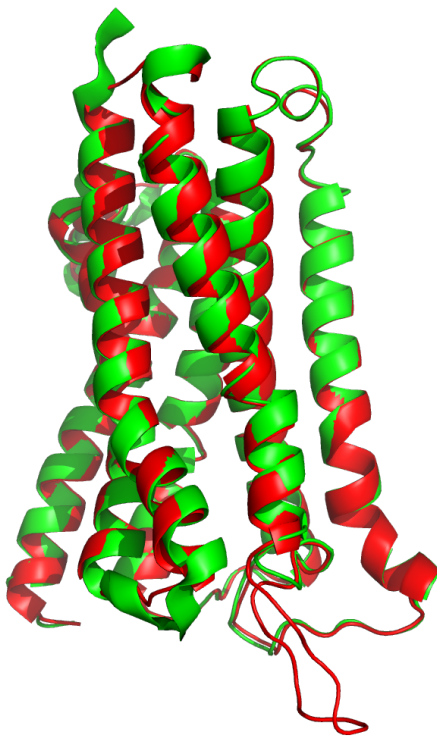


Fig. S1. OR2M3 modeled 3-dimensional structure and its template.

Sequence alignment of the seven TMH regions of the homology model of OR2M3 (red) with the human M1 muscarinic receptor (5CXV.pdb, green).

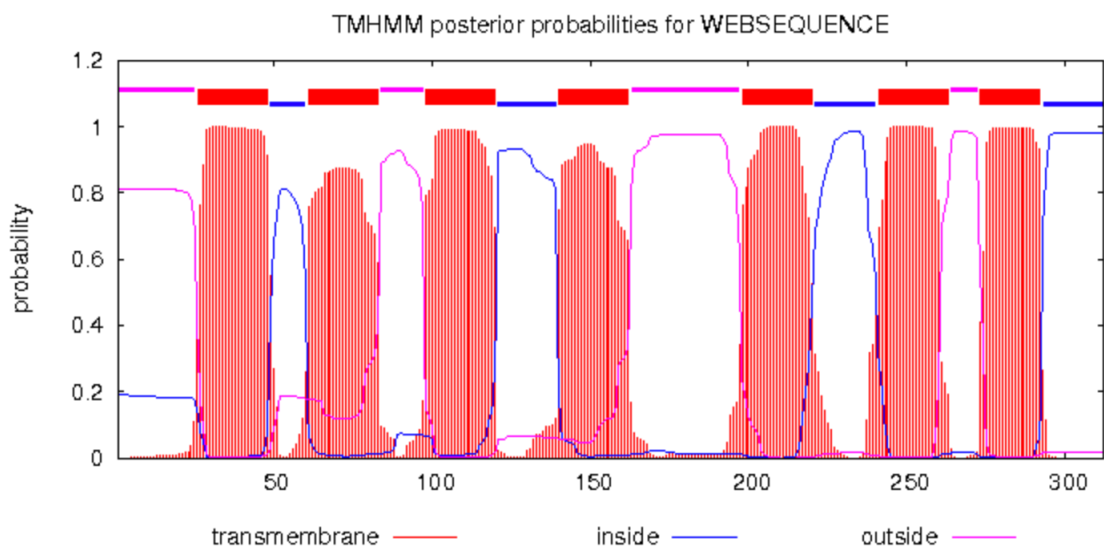


Fig. S2. TMHMM posterior probabilities for OR2M3.

The graphical output of TMHMM shows the posterior probabilities for transmembrane, inside, and outside regions. Transmembrane regions are indicated as red bars.

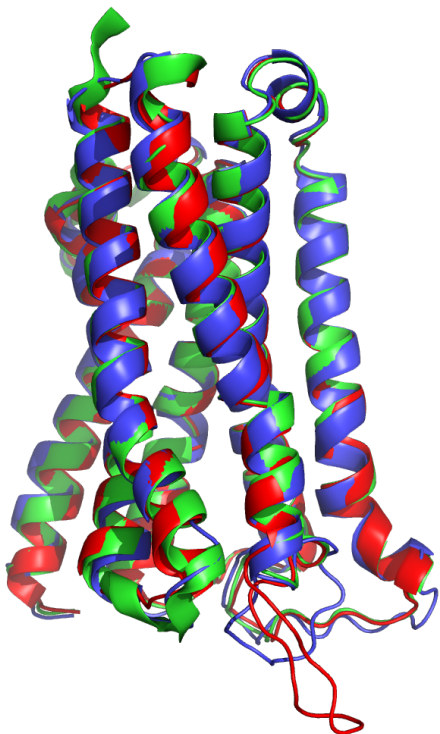


Fig. S3. OR2W1 and OR2M3 modeled 3-dimensional structures and their template.

Sequence alignment of the seven TMH regions of the homology model of OR2M3 (red) and OR2W1 (blue) with the human M1 muscarinic receptor (5CXV.pdb, green).

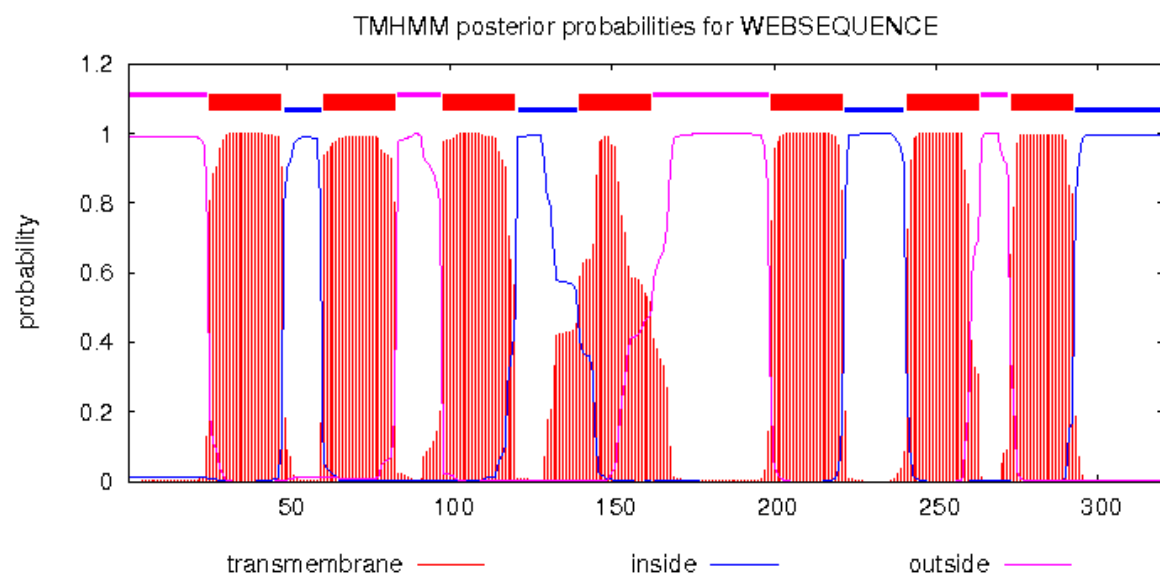


Fig. S4. TMHMM posterior probabilities for OR2W1.

The graphical output of TMHMM shows the posterior probabilities for transmembrane, inside, and outside regions. Seven transmembrane regions are indicated as red bars.

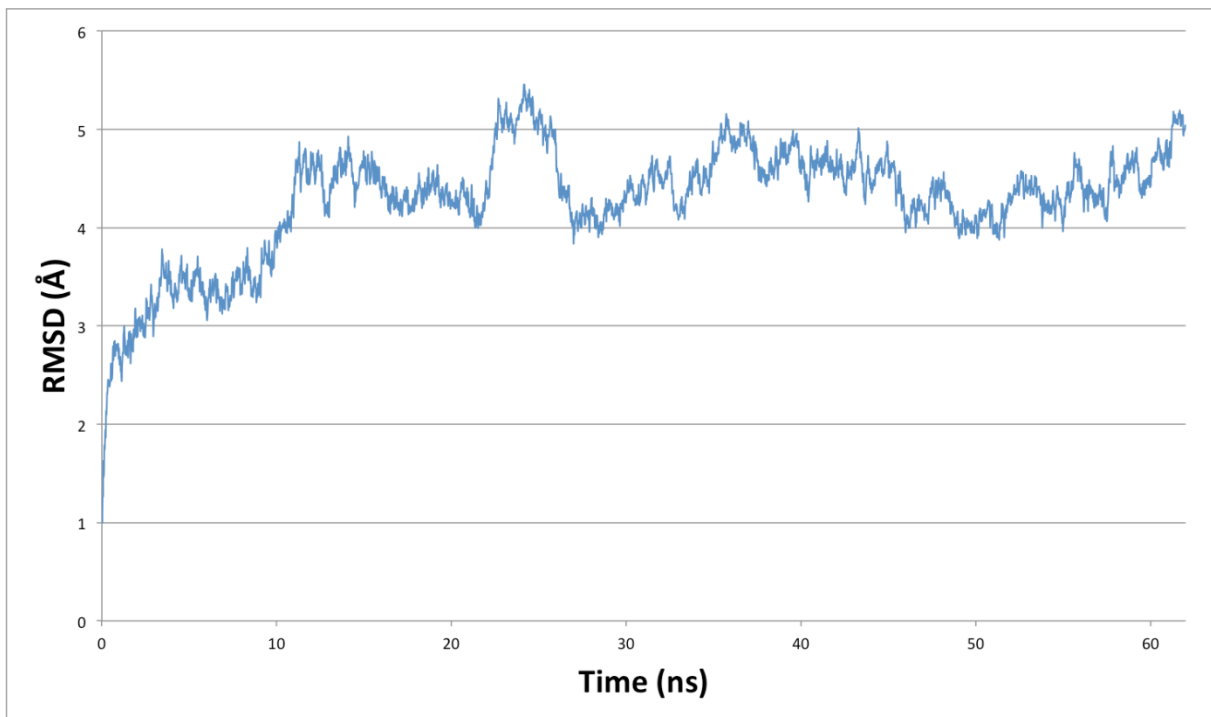


Fig. S5. C(α)-RMSD plot of OR2W1.

Shown is a 62 ns simulation of OR2W1 in a water box without a membrane, which stabilizes to $\sim 4.5 \text{ \AA}$ after the first 12 ns.

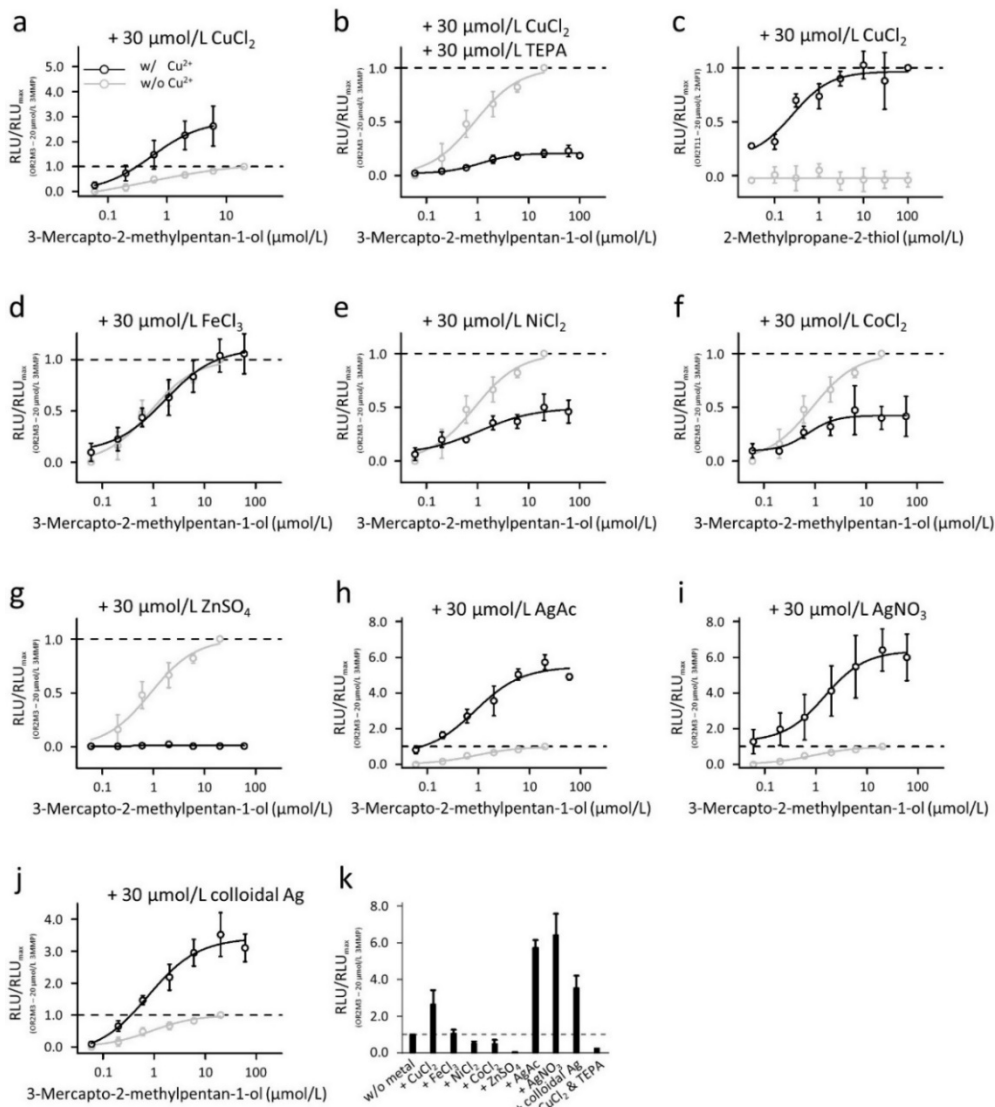


Fig. S6. Copper and silver enhance the 3-mercaptopentan-1-ol efficacy on OR2M3.

Concentration-response relation of 3-mercaptopentan-1-ol on OR2M3 in the absence or presence of each 30 μmol/L CuCl₂ (a), and 30 μmol/L CuCl₂ and the copper chelator TEPA (b). Concentration-response relation of 2-methylpropane-2-thiol on OR2T11 C₁₁₉R in the absence or presence of 30 μmol/L CuCl₂ (c). Concentration-response relation of 3-mercaptopentan-1-ol on OR2M3 in the absence or presence of each 30 μmol/L FeCl₃ (d); NiCl₂ (e); CoCl₂ (f); ZnSO₄ (g); AgAc (h); AgNO₃ (i) and colloidal silver (j). Comparison of efficacies of 20 μmol/L 3-mercaptopentan-1-ol on OR2M3 in the absence or presence of different metal ions at 30 μmol/L (k). Note that the same data set in the absence of supplemented Cu²⁺ (grey) is given in sub-panels (a-b, d-j) for didactic reasons. Data were mock control-subtracted, normalized to the OR2M3 wt signal in response to 3-mercaptopentan-1-ol (20 μmol/L), measured in the absence of Cu²⁺ (a-b, d-k) or rather normalized to the OR2T11 C₁₁₉R signal in response to 2-methylpropane-2-thiol (100 μmol/L), measured in the presence of Cu²⁺ (c), and shown as mean ± SD ($n = 3 - 6$). RLU = relative luminescence unit. 3MMP = 3-mercaptopentan-1-ol. Curves represent best fits to the data in the absence (grey) or presence (black) of Cu²⁺, with EC₅₀ values given in Table S6. Note that for didactical reasons the concentration-response relations in Fig. 1b and Fig. S5a are the identical data set. Also Fig. 1a and Fig. S5k are the identical data set.

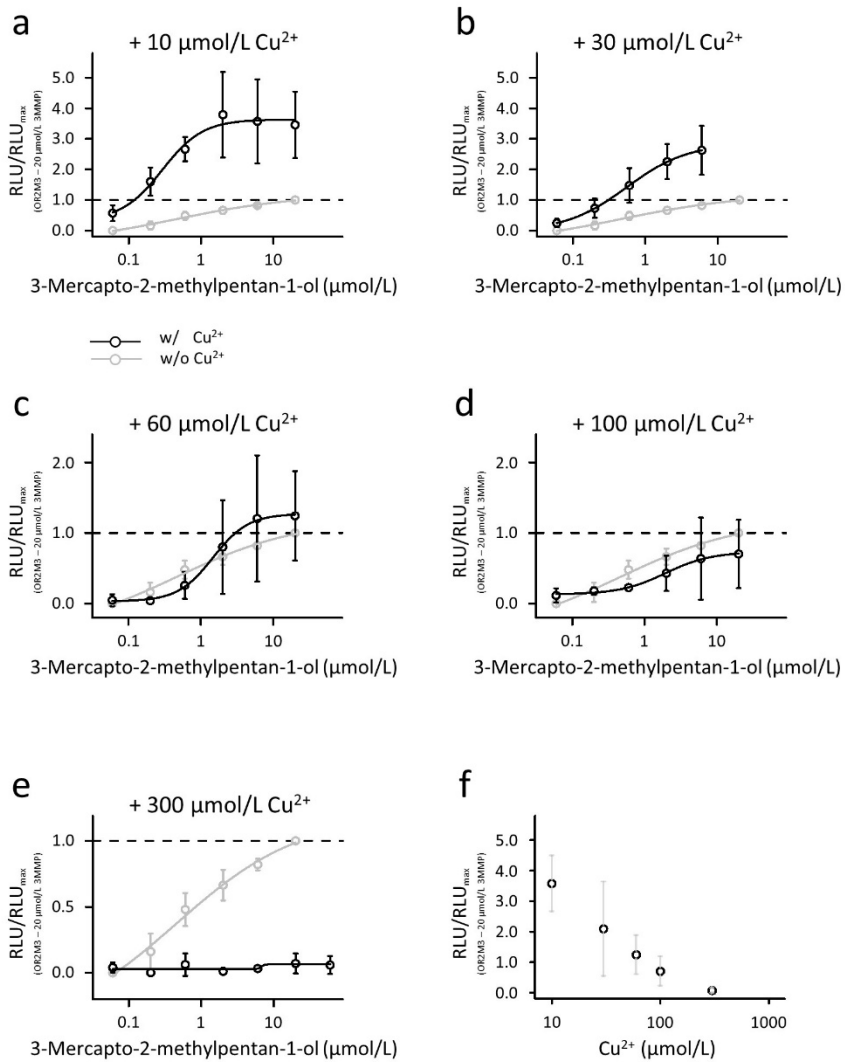


Fig. S7. The strongest increase in efficacy of 3-mercaptopentan-1-ol on OR2M3 was observed with 10 $\mu\text{mol/L}$ Cu^{2+} .

Concentration-response relation of 3-mercaptopentan-1-ol on OR2M3 in the absence or presence of 10 $\mu\text{mol/L}$ CuCl_2 (a); 30 $\mu\text{mol/L}$ CuCl_2 (b); 60 $\mu\text{mol/L}$ CuCl_2 (c); 100 $\mu\text{mol/L}$ CuCl_2 (d) and 300 $\mu\text{mol/L}$ CuCl_2 (e). Comparison of efficacies of 20 $\mu\text{mol/L}$ 3-mercaptopentan-1-ol on OR2M3 with different Cu^{2+} concentrations in ascending order (f). Note that the same data set in the absence of supplemented Cu^{2+} (grey) is given in sub-panels (a-e) for didactic reasons. Data were mock control-subtracted, normalized to the OR2M3 wt signal in response to 3-mercaptopentan-1-ol (20 $\mu\text{mol/L}$), measured in the absence of Cu^{2+} , and shown as mean \pm SD ($n = 3 - 6$). RLU = relative luminescence unit. 3MMP = 3-mercaptopentan-1-ol. Curves represent best fits to the data in the absence (grey) or presence (black) of Cu^{2+} , with EC₅₀ values given in Table S7. Note that for didactical reasons, the concentration-response relations in Fig. 1d and Fig. S6a, as well as sub-panels Fig. 1c and Fig. S6f, are the identical data set.

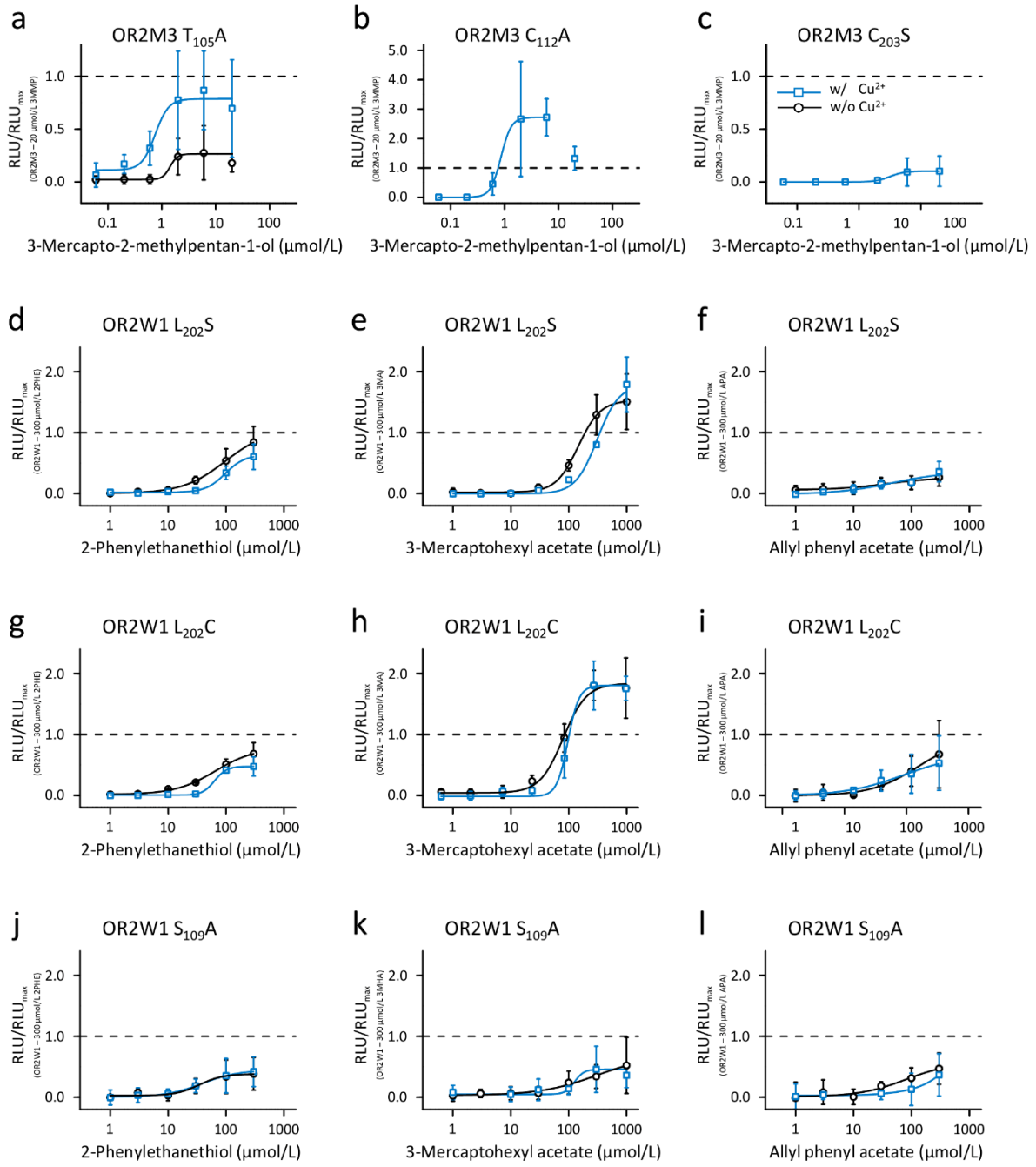


Fig. S8. Cu²⁺ influences the efficacy of 3-mercaptopentan-1-ol on OR2M3 but not of OR2W1 agonists.

Effects of 10 μmol/L Cu²⁺ on the concentration-response relations of 3-mercaptopentan-1-ol of OR2M3 variants (a, b, c), 2-phenylethanethiol of OR2W1 variants (d, g, j), 3-mercaptobhexyl acetate of OR2W1 variants (e, h, k), and allyl phenyl acetate of OR2W1 variants (f, i, l). Data were mock control-subtracted, normalized to each receptor maximum amplitude as response to the respective substance measured in the absence of Cu²⁺, and shown as mean ± SD (n = 3 – 6). RLU = relative luminescence unit. Curves represent best fits to the data in the absence (black) or presence (blue) of Cu²⁺, with EC₅₀ values given in Table 4. 3MMP = 3-mercaptopentan-1-ol, 2PHE = 2-phenylethanethiol, 3MAc = 3-mercaptobhexyl acetate, APA = allyl phenyl acetate.

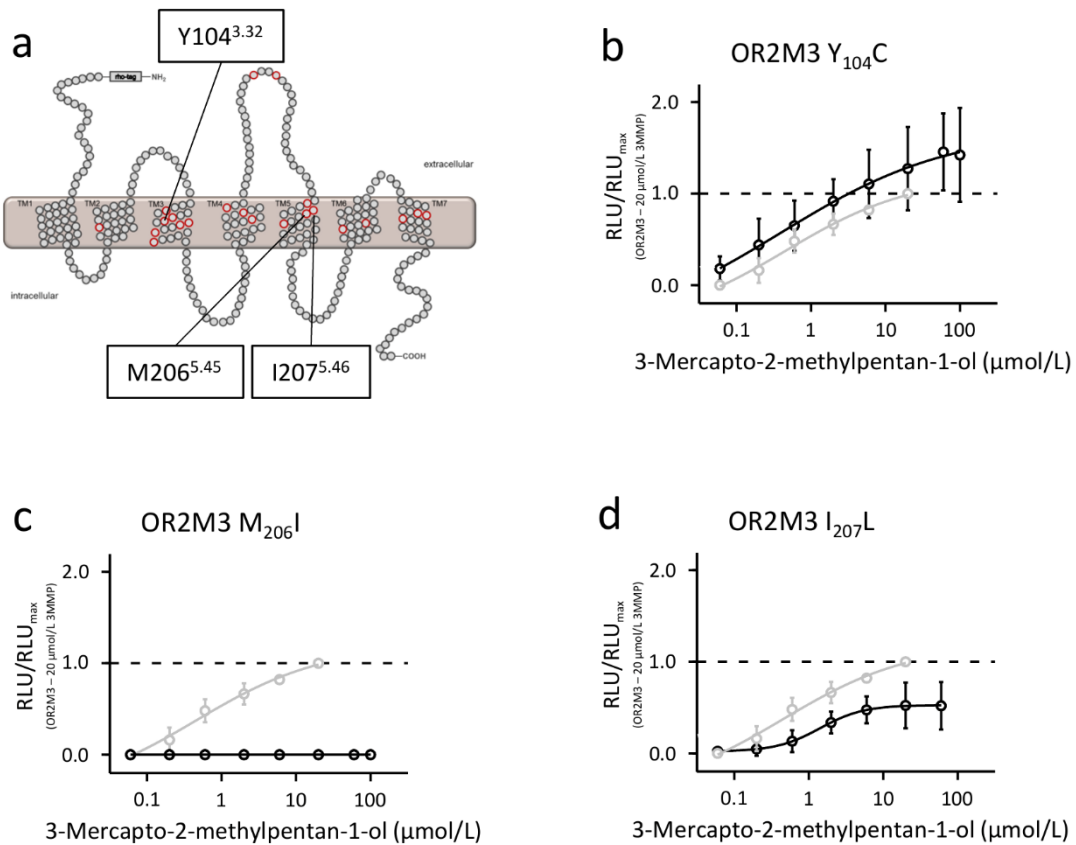


Fig. S9. SNP-defined OR2M3 haplotypes display 3-mercaptopentan-1-ol gain- and loss-of-function phenotypes.

(a) Schematic snake diagram with localization of mutated amino acid positions within OR2M3, which have been chosen because of their close vicinity to putative interaction sites with odorants as proposed by Man et al. [80] (red circles). Effects of 3-mercaptopentan-1-ol on OR2M3 variants (black curves) with SNP-defined single amino acid changes at positions 104^{3.32} (b), 206^{5.45} (c), and 207^{5.46} (d). Note that the same data set for 3-mercaptopentan-1-ol on OR2M3 wt (grey, see also Fig. 1b, d) is given in panels (b)-(d) for didactic reasons. EC₅₀ values are given in Table 3. Data were mock control-subtracted, normalized to OR2M3 wt maximum amplitude, and displayed as mean ± SD (n = 3 – 6). RLU = relative luminescence unit. 3MMP = 3-mercaptopentan-1-ol.

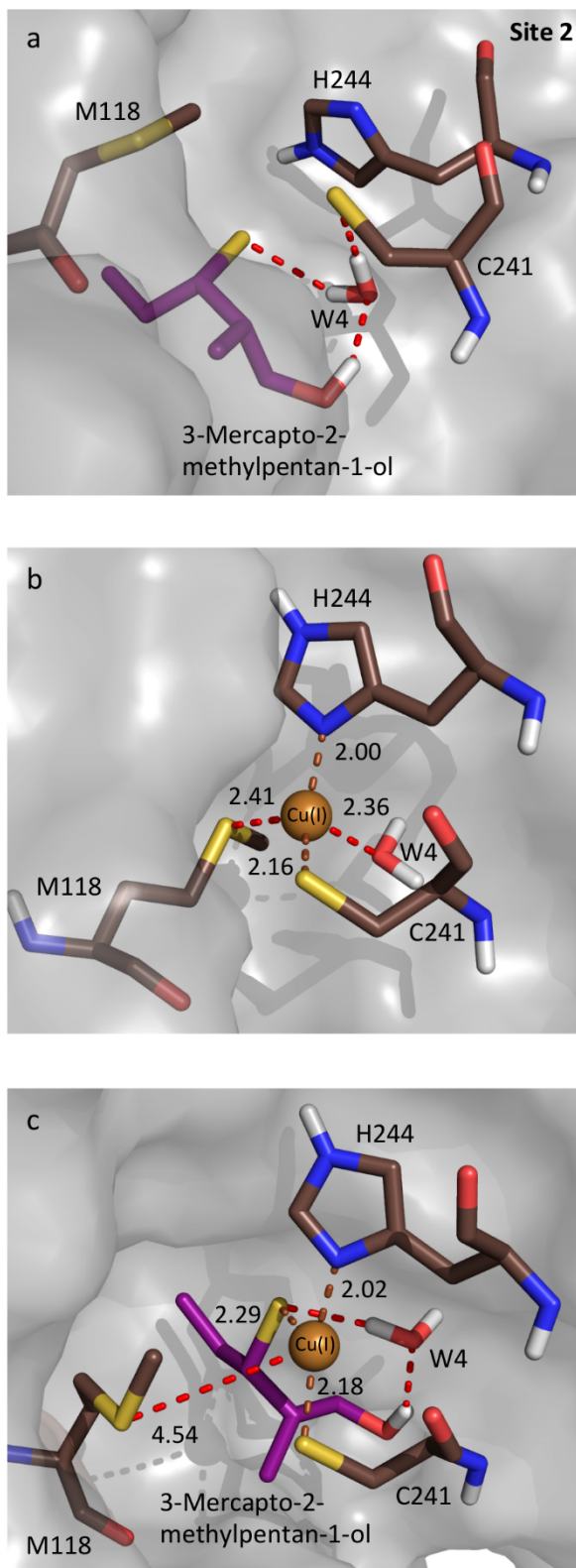


Fig S10. Molecular models of the ligand and copper binding cavity for OR2M3.

QM/MM structural model of site 2 in OR2M3 with the ligand 3-mercaptopentan-1-ol (a), with Cu(I) (b), or both (c). Residues defining the binding pocket are shown as sticks (oxygen: red; nitrogen: blue; sulfur: yellow).

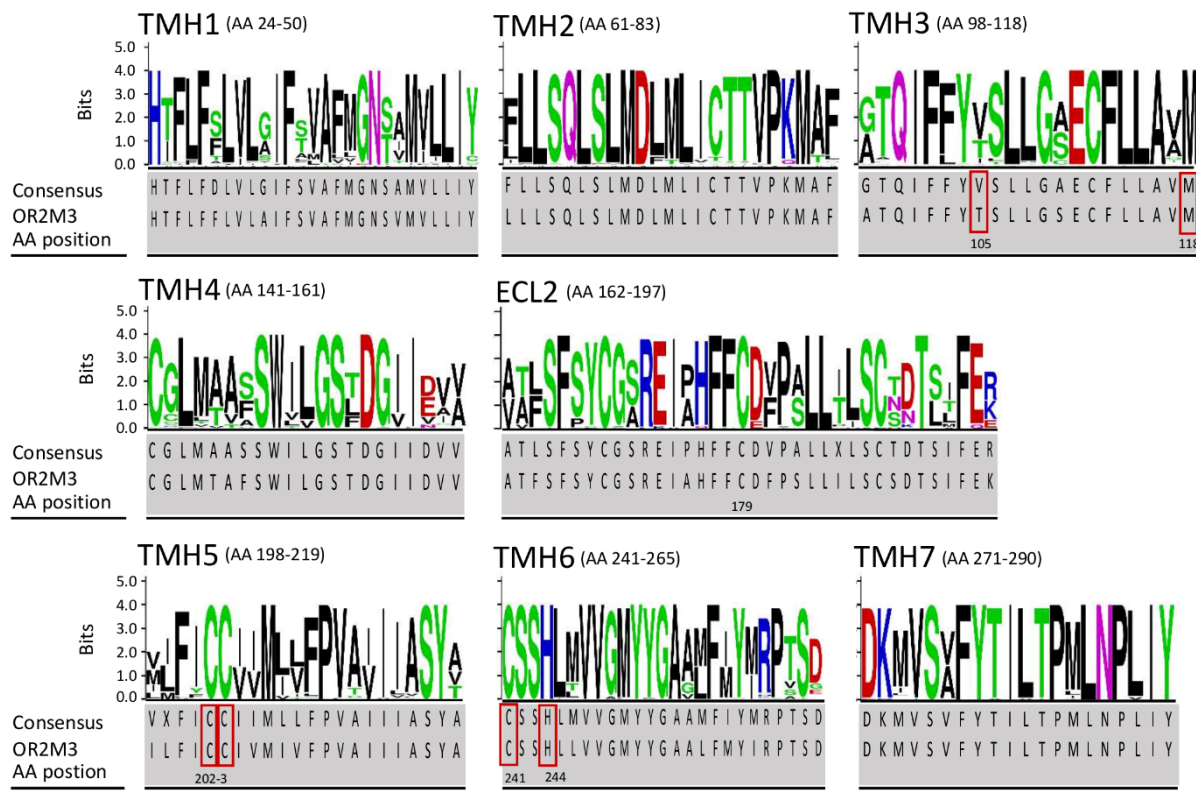


Fig. S11. A conserved copper binding motif within OR2M3 homologs.

Alignments of transmembrane helices (TMH 1 – 7) and extracellular loop 2 (ECL 2) of human OR2M3 and its 47 orthologs and paralogs. Shown are sequence logos, the consensus sequence, and the human OR2M3 sequence with the 3-mercaptop-2-methylpentan-1-ol and copper binding pocket (red boxes). The consensus amino acid refers to the most frequent one, which is determined by letter height and stacking order. The letters of each stack are ordered from the most frequent to the least frequent. Amino acid conservation is measured in bits, and a 100% conservation correlates to 4.32 bits [4]. Basic amino acids (K, R, H) are blue, polar (G, S, T, Y C) are green, hydrophilic (Q, N) are purple, acidic (D, E) are red, and hydrophobic (A, V, L, I, P, W, M, F) are black. All reference sequences with their accession numbers are given in Table S5.

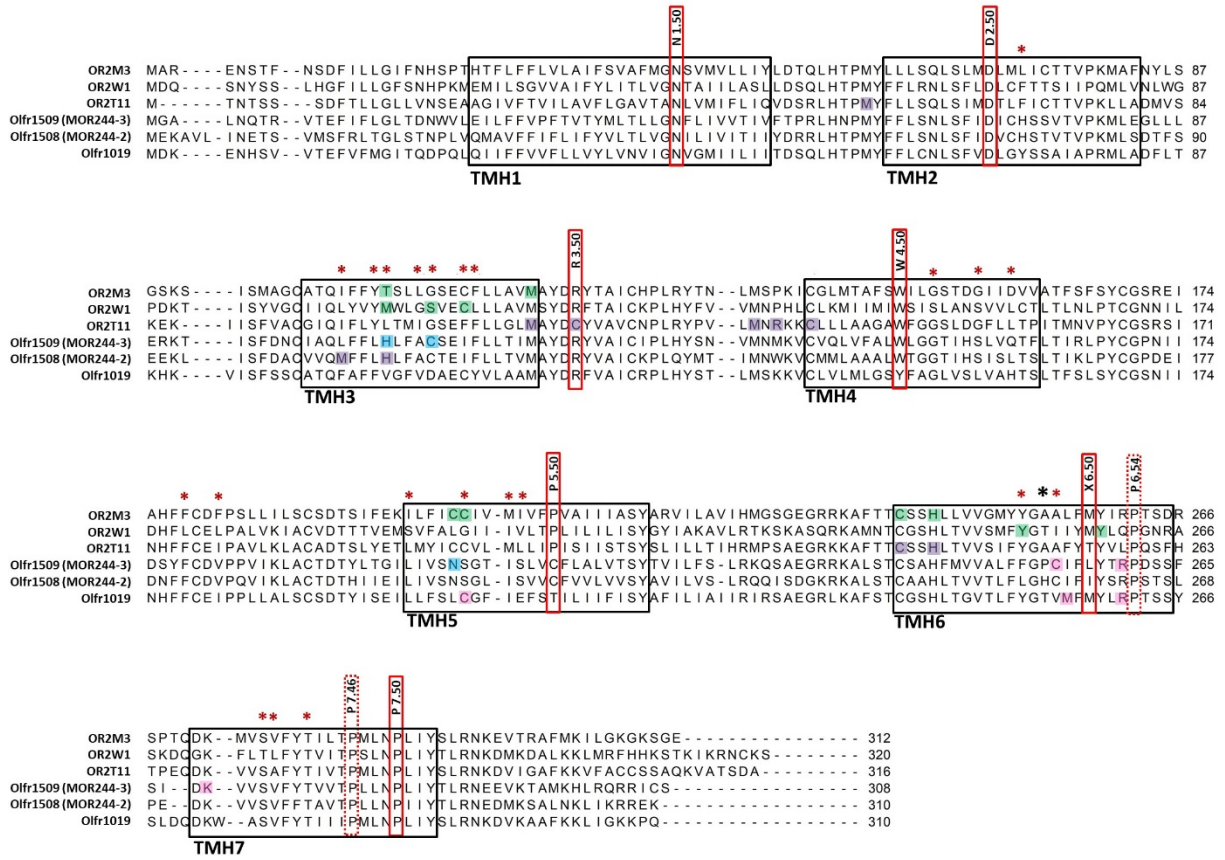


Fig. S12. Copper binding site within different ORs.

Shown is the sequence alignment (CLC Main Workbench 6.5) of ORs which were previously investigated by different working groups [5-7]. The respectively identified amino acids of the copper binding site are highlighted with color boxes (see color coding). The transmembrane helices (TMHs) are indicated as black boxes. According to the Ballesteros-Weinstein nomenclature the highly conserved amino acid within each TMH is given the number '50' [8]. The 22 amino acid residues according to Man *et al.* [1] are marked with red asterisk. The black asterisk in TMH 6 refers to X6.50 according to de March *et al.* [9, 10].

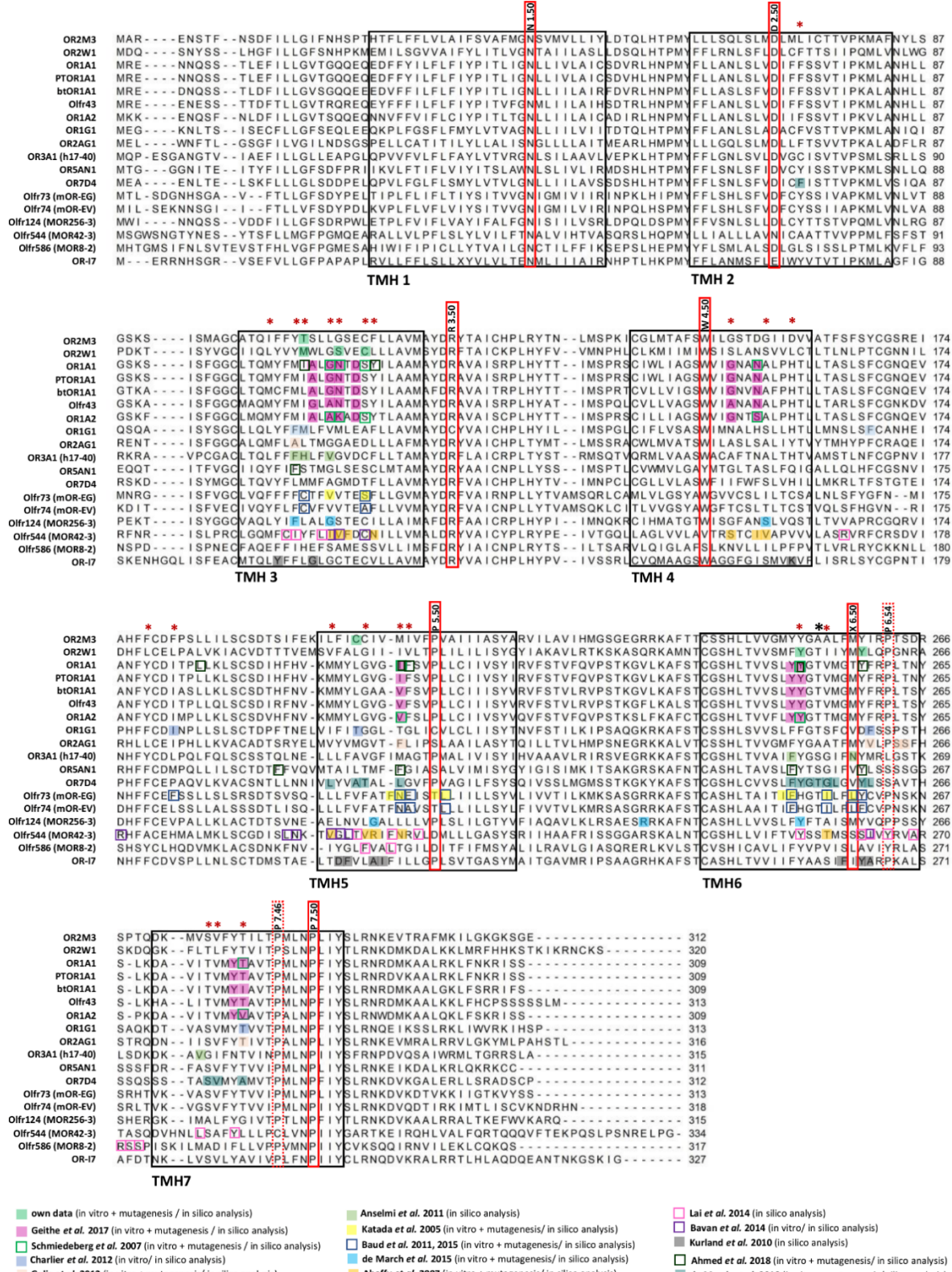


Fig. S13. Odorant binding site within different ORs.

Shown is the sequence alignment (CLC Main Workbench 6.5) of ORs which were previously investigated by different working groups [10-24]. The respectively identified amino acids of the odorant binding site were highlighted with color boxes (see color coding). The transmembrane helices (TMHs) are indicated as black boxes. According to the Ballesteros-Weinstein nomenclature the highly conserved amino acid within each TMH was given the number '50' [8]. The 22 amino acid residues according to Man *et al.* [1] were marked with red asterisk. The black asterisk in TMH 6 refers to X6.50 according to de March *et al.* [9, 10].

Measuring cell surface expression of OR2M3 and its variants by using flow cytometry

NxG 108CC15 cells [25] were cultivated in 12-well plates (80 000 cells/well) and transiently transfected with 800 ng plasmid DNA (pI2-dk - 39AA rho-tag + HaloTag®) of the respective odorant receptor (OR) variant as well as 400 ng plasmid DNA of Gaolf, Gy13, RTP1S and cAMP-luciferase pGloSensor™-22F each using Lipofectamine® 2000 (Life Technologies, Carlsbad, USA). To keep the amount of transfected DNA compared to cell number the same as in the luminescence assay, we also transfected the cAMP-luciferase pGloSensor™-22F, although it has no impact on cell surface expression of the respective OR. Basically, the experimental settings were scaled up 8-fold from the 96-well luminescence assay to the 12-well flow cytometry assay. The rho-tagged OR were additionally fused with a HaloTag® (Promega, Madison, USA) [26] which is suitable for the detection by fluorescence labeled ligands via flow cytometry.

We used the membrane non-permeable ligand HaloTag® AlexaFluor 488 (ex/em = 499/518 nm) and the membrane permeable HaloTag® TMR ligand (ex/em = 552/578 nm) from Promega, Madison, USA. For analysis, cells were harvested 42 h post transfection and stained for 1 hour either with HaloTag® AlexaFluor 488 ligand or HaloTag® TMR ligand at 37°C, 7% CO₂ and 100 % humidity. Afterwards, the cells were washed twice with serum free medium prior flow cytometry analysis (MACSQuant Analyzer, Milteny Biotec, Bergisch Gladbach, Germany). For the HaloTag® TMR ligand, an additional incubation step in growth medium for 30 min at 37°C, 7% CO₂ and 100 % humidity was necessary.

A forward- and side-scatter gate was set to exclude dead cells with forward-scatter (FSC: 235V) and side-scatter (SSC: 360V). The FITC signal (B1-channel; HaloTag® Alexa Fluor488 ligand was detected with 190V and the PE signal (B2-channel, HaloTag® TMR ligand) with 416V. In each case 10,000 cells were measured. The analysis was performed with the MACSQuantify software (Milteny Biotec, Bergisch Gladbach, Germany). The FITC or PE signal of each mock-control defined the distinction between negative and positive cells.

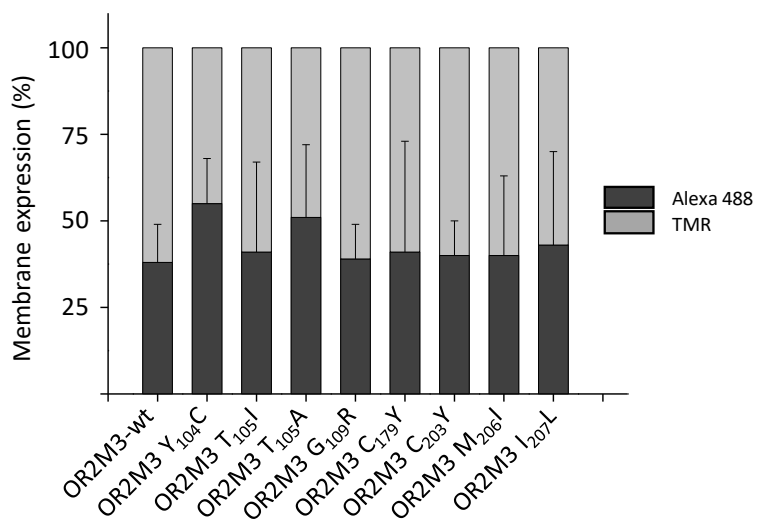


Fig. S14: Cell surface expression of OR2M3 wt and variants.

Shown are mean ± SD (n=3-6). The data represents the percentage of relative membrane expression of OR-transfected NxG cells determined by membrane non-permeable HaloTag® AlexaFluor 488 ligand (dark grey bars) compared to membrane permeable HaloTag® TMR ligand (light grey bars). wt, NCBI reference sequence.

Supplemental Literature

1. Man O, Gilad Y, Lancet D (2004) Prediction of the odorant binding site of olfactory receptor proteins by human-mouse comparisons. *Protein Sci* 13 (1):240-254.
2. Genomes Project C, Abecasis GR, Altshuler D, Auton A, Brooks LD, Durbin RM, Gibbs RA, Hurles ME, McVean GA (2010) A map of human genome variation from population-scale sequencing. *Nature* 467 (7319):1061-1073.
3. Sherry ST, Ward MH, Kholodov M, Baker J, Phan L, Smigielski EM, Sirotnik K (2001) Dbsnp: The ncbi database of genetic variation. *Nucleic Acids Res* 29 (1):308-311.
4. Crooks GE, Hon G, Chandonia J-M, Brenner SE (2004) Weblogo: A sequence logo generator. *Genome Research* 14 (6):1188-1190.
5. Sekharan S, Ertem MZ, Zhuang H, Block E, Matsunami H, Zhang R, Wei JN, Pan Y, Batista VS (2014) Qm/mm model of the mouse olfactory receptor mor244-3 validated by site-directed mutagenesis experiments. *Biophys J* 107 (5):L5-L8.
6. Li S, Ahmed L, Zhang R, Pan Y, Matsunami H, Burger JL, Block E, Batista VS, Zhuang H (2016) Smelling sulfur: Copper and silver regulate the response of human odorant receptor or2t11 to low-molecular-weight thiols. *J Am Chem Soc*.
7. Zhang R, Pan Y, Ahmed L, Block E, Zhang Y, Batista VS, Zhuang H (2018) A multispecific investigation of the metal effect in mammalian odorant receptors for sulfur-containing compounds. *Chem Senses* 43 (5):357-366.
8. Ballesteros JA, Weinstein H (1995) Integrated methods for the construction of three-dimensional models and computational probing of structure-function relations in g protein-coupled receptors. In: Sealfon SC (ed) *Methods in neurosciences*, vol 25. Academic Press, pp 366-428.
9. de March CA, Kim SK, Antonczak S, Goddard WA, 3rd, Golebiowski J (2015) G protein-coupled odorant receptors: From sequence to structure. *Protein Sci* 24 (9):1543-1548.
10. de March CA, Yu Y, Ni MJ, Adipietro KA, Matsunami H, Ma M, Golebiowski J (2015) Conserved residues control activation of mammalian g protein-coupled odorant receptors. *J Am Chem Soc* 137 (26):8611-8616.
11. Geithe C, Protze J, Kreuchwig F, Krause G, Krautwurst D (2017) Structural determinants of a conserved enantiomer-selective carvone binding pocket in the human odorant receptor or1a1. *Cell Mol Life Sci* 74 (22):4209-4229.
12. Schmiedeberg K, Shirokova E, Weber HP, Schilling B, Meyerhof W, Krautwurst D (2007) Structural determinants of odorant recognition by the human olfactory receptors or1a1 and or1a2. *J Struct Biol* 159 (3):400-412.
13. Gelis L, Wolf S, Hatt H, Neuhaus EM, Gerwert K (2012) Prediction of a ligand-binding niche within a human olfactory receptor by combining site-directed mutagenesis with dynamic homology modeling. *Angew Chem Int Ed Engl* 51 (5):1274-1278.
14. Katada S, Hirokawa T, Oka Y, Suwa M, Touhara K (2005) Structural basis for a broad but selective ligand spectrum of a mouse olfactory receptor: Mapping the odorant-binding site. *J Neurosci* 25 (7):1806-1815.
15. Baud O, Etter S, Spreafico M, Bordoli L, Schwede T, Vogel H, Pick H (2011) The mouse eugenol odorant receptor: Structural and functional plasticity of a broadly tuned odorant binding pocket. *Biochemistry* 50 (5):843-853.
16. Abaffy T, Malhotra A, Luetje CW (2007) The molecular basis for ligand specificity in a mouse olfactory receptor: A network of functionally important residues. *J Biol Chem* 282 (2):1216-1224.

17. Lai PC, Crasto CJ (2012) Beyond modeling: All-atom olfactory receptor model simulations. *Front Genet* 3:61.
18. Anselmi C, Buonocore A, Centini M, Facino RM, Hatt H (2011) The human olfactory receptor 17-40: Requisites for fitting into the binding pocket. *Comput Biol Chem* 35 (3):159-168.
19. Bavan S, Sherman B, Luetje CW, Abaffy T (2014) Discovery of novel ligands for mouse olfactory receptor mor42-3 using an in silico screening approach and in vitro validation. *PLoS One* 9 (3):e92064.
20. Kurland MD, Newcomer MB, Peterlin Z, Ryan K, Firestein S, Batista VS (2010) Discrimination of saturated aldehydes by the rat i7 olfactory receptor. *Biochemistry* 49 (30):6302-6304.
21. Baud O, Yuan S, Veya L, Filipek S, Vogel H, Pick H (2015) Exchanging ligand-binding specificity between a pair of mouse olfactory receptor paralogs reveals odorant recognition principles. *Scientific Reports* 5:14948.
22. Charlier L, Topin J, Ronin C, Kim SK, Goddard WA, 3rd, Efremov R, Golebiowski J (2012) How broadly tuned olfactory receptors equally recognize their agonists. Human or1g1 as a test case. *Cell Mol Life Sci* 69 (24):4205-4213.
23. Ahmed L, Zhang Y, Block E, Buehl M, Corr MJ, Cormanch RA, Gundala S, Matsunami H, O'Hagan D, Ozbil M, Pan Y, Sekharan S, Ten N, Wang M, Yang M, Zhang Q, Zhang R, Batista VS, Zhuang H (2018) Molecular mechanism of activation of human musk receptors or5an1 and or1a1 by (r)-muscone and diverse other musk-smelling compounds. *Proc Natl Acad Sci U S A* 115 (17):E3950-E3958.
24. de March CA, Topin J, Bruguera E, Novikov G, Ikegami K, Matsunami H, Golebiowski J (2018) Odorant receptor 7d4 activation dynamics. *Angew Chem Int Ed Engl* 57 (17):4554-4558.
25. Hamprecht B, Glaser T, Reiser G, Bayer E, Propst F (1985) Culture and characteristics of hormone-responsive neuroblastoma x glioma hybrid cells. *Methods Enzymol* 109:316-341.
26. Los GV, Encell LP, McDougall MG, Hartzell DD, Karassina N, Zimprich C, Wood MG, Learish R, Ohana RF, Urh M, Simpson D, Mendez J, Zimmerman K, Otto P, Vidugiris G, Zhu J, Darzins A, Klaubert DH, Bulleit RF, Wood KV (2008) Halotag: A novel protein labeling technology for cell imaging and protein analysis. *ACS Chem Biol* 3 (6):373-382.